REVIEW

Application of flash nanoprecipitation to fabricate poorly water-soluble drug nanoparticles ☆

Jinsong Tao[a], Shing Fung Chow[b], Ying Zheng[a,*]

[a]State Key Laboratory of Quality Research in Chinese Medicine, Institute of Chinese Medical Science, University of Macau, Macau, China
[b]Department of Pharmacology and Pharmacy, The University of Hong Kong, Hong Kong, China

Abstract Nanoparticles are considered to be a powerful approach for the delivery of poorly water-soluble drugs. One of the main challenges is developing an appropriate method for preparation of drug nanoparticles. As a simple, rapid and scalable method, the flash nanoprecipitation (FNP) has been widely used to fabricate these drug nanoparticles, including pure drug nanocrystals, polymeric micelles, polymeric nanoparticles, solid lipid nanoparticles, and polyelectrolyte complexes. This review introduces the application of FNP to produce poorly water-soluble drug nanoparticles by controllable mixing devices, such as confined impinging jets mixer (CIJM), multi-inlet vortex mixer (MIVM) and many other microfluidic mixer systems. The formation mechanisms and processes of drug nanoparticles by FNP are described in detail. Then, the controlling of supersaturation level and mixing rate during the FNP process to tailor the ultrafine drug nanoparticles as well as the influence of drugs, solvent, anti-solvent, stabilizers

and temperature on the fabrication are discussed. The ultrafine and uniform nanoparticles of poorly water-soluble drug nanoparticles prepared by CIJM, MIVM and microfluidic mixer systems are reviewed briefly. We believe that the application of microfluidic mixing devices in laboratory with continuous process control and good reproducibility will be benefit for industrial formulation scale-up.

1. Introduction

High throughput screening for drug discovery often generates many lipophilic active pharmaceutical ingredients (APIs), which requires formulation scientist to address their poor aqueous solubility and dissolution. According to the biopharmaceutics classification system (BCS), more than 40% of the drugs fall in the BCS Class II (low solubility-high permeability) and Class IV (low solubility-low permeability) categories[1]. Depending on drug physicochemical property and chemical structure, although many formulation strategies, including complexing drugs with cyclodextrins[2], conjugating drug to dendrimers[3], salt formation of ionizable drugs[4], prodrugs[5], solid dispersions[6] and use of co-solvents[7], have demonstrated the improved drug solubility and dissolution, a universal solubilization technique which is suitable for most of the lipophilic drugs are still highly desirable[8]. A growing interest has been focused on nanoscience and nanotechnology in medicine, where the nanodrug delivery systems were viewed as nanocarriers loaded with APIs in a scale range up to 1000 nm. The API was stabilized with excipients to form drug nanoparticle dispersion systems, such as micelles, polymeric nanoparticles, nanocrystals, nanoemulsions, liposomes and mesoporous silica nanoparticles[9]. These nanoparticle formulations provided several advantages for the delivery of insoluble drugs, including: (1) the drug nanoparticles could increase the surface area to volume ratio, which generally improves the dissolution rate and solubility of poorly water-soluble drugs[10], enhance specific interactions with cells and tissues, promote absorption and enhance bioavailability for BCS class II drugs[11,12]; (2) formulation as nanodrugs will enhance the chemical stability of some drugs and control their release profile in gastrointestinal tract; (3) the drug nanoparticles could be tailored *via* surface functionality to achieve long circulation and targeted delivery[13,14].

The fabrication techniques of drug nanoparticles are mainly divided into top-down and bottom-up methods[15]. The top-down methods start with large drug solid crystals, which will be mechanically broken down into nanometer scaled drug particles by media milling or high-pressure homogenization. Particle size reduction with these methods is mainly obtained by shear, attrition, friction, pressure, or any combination. The top-down methods are able to produce fine drug nanoparticles and are viable for industrial scale-up production. Extensive studies have proven that these methods are effective for reproducible production of particles in the size range of a few hundred nanometers to 2 μm with the aid of proper stabilizers[16,17]. However, it is extremely tough to break drug particles size down to 100 nm with these top-down methods[18]. Moreover, the top-down methods is time and energy consuming, and the contamination from milling material or homogenization chamber is also a concern. On the contrary, the bottom-up methods including nanoprecipitation[19,20], evaporation[21], salting-out[22], supercritical fluid technique[23,24], and emulsification[25] method are far more utilized in research laboratories because they could prepare smaller nanoparticles than top-down methods without requiring expensive equipment. Among of them, flash nanoprecipitation (FNP) provides a rapid mixing process based on kinetically controlled nanoprecipitation to tailor the size and surface properties of nanoparticles through the formulation of unique composition with stabilizers. It is relatively easy to scale up, efficient and reproducible for industrial use compared to other bottom-up methods. Therefore, this review will focus on introduction of FNP, such as the principle, mixing device, formulation of nanoparticles and application on poorly water-soluble drug nanoparticle formulations.

Fabrication of drug nanoparticles by FNP were suitable for poorly water-soluble drugs *via* the stabilizing nanoparticles surface by stabilizers, such as surfactants, polymers, and lipids, which were widely used to tailor the size of the nanoparticles. At present in laboratories, nanoparticles are mainly produced in a batch mode, although batch fabrication tends to suffer from irreproducibility of size, size distribution, and quality of the nanoparticles from batch to batch. It is critical to have an efficient, reproducible and controllable fabrication technique of nanoparticles *via* FNP. Therefore, several microfluidic mixing devices were developed to produce nanoparticles of poorly water-soluble drugs with continuous process control and excellent reproducibility. The most popular and successful microfluidic mixing devices reported were confined impinging jets mixer (CIJM) developed by Johnson and Prud'homme[26–28] and multi-inlet vortex mixer (MIVM) by Liu and Prud'homme[29]. For further development with more convenient in tiny scale, various microfluidic mixer systems were also explored[20,30,31].

2. Flash nanoprecipitation (FNP)

2.1. Principles

FNP is widely used to tailor-made drug nanoparticles (*i.e.*, aqueous nanosuspension of poorly water-soluble drugs) through bottom-up approach. As with conventional crystallization process, nanoparticles formed by FNP involve an initial nucleation stage, then the newly formed nucleation seeds capture dissolved molecules to grow up. The classical crystallization theory of molecule is a useful model to understand the mechanism of NPs

formation by FNP[32]. It involves a phase separation of solid from liquid process which is thermodynamically favorable. The driving force of such phase separation is the reduction from the high free energy (ΔG) of the supersaturation to nanoparticle suspension which has low ΔG and is thermodynamically stable. According to this theory, the nucleation mechanisms have be divided as "homogenous nucleation" which is in absence of foreign substance, and "heterogeneous nucleation" with existing foreign substance[33]. For the drug nanoparticles prepared by FNP, their nucleation mechanisms were considered to be coexistence of homogeneous nucleation and heterogeneous nucleation[34]. The primary nucleation in FNP was likely to be heterogeneous nucleation, because supersaturation required for homogeneous nucleation was much higher than heterogeneous nucleation. Actually, the homogeneous nucleation of drug nucleus may start firstly due to higher supersaturation rate and higher nucleation rate of drug molecule. For heterogeneous nucleation in FNP process, the nucleus is the matrix of drug molecules and/or other hydrophobic excipients for the formation of nanocrystals, micelles, polymeric nanoparticles or solid lipid nanoparticles. The hydrophobic sites served as the nucleation seeds. The formed seeds could reduce the critical free energy (ΔG_{cr}) for nucleation formulation and thus nucleation of solute occurs at a lower supersaturation condition. Therefore, the heterogeneous nucleation is much easier than homogeneous nucleation which is dominant in the FNP process.

The precipitation of nanoparticles process involves a rapid impingement mixing of two or more miscible liquid in a confined chamber, which include the following steps: solution and anti-solvent flash mixed to create high supersaturation condition, triggering solute (drug) nucleation, and growth by coagulation and condensation, simultaneously stabilized by precipitation of lipids, polymers or/and surfactants, to control the particle size in nanometer. The lipids, polymers or/and surfactants encapsulate drug molecule into hydrophobic core and provide steric stabilization by the hydrophilic layer around the nanoparticles, that inhibit further growth and aggregation of the nanoparticles.

The process of FNP contains several key components, the first of which is a rapid mixing time to create high supersaturation. The supersaturation for nanoprecipitation in solution is defined in Eq. (1):

$$S = C/C^* \tag{1}$$

where C represents real time concentration of drug in the organic solvent and anti-solvent mixture and C^* represents the saturation solubility of drug in the mixed solution. As shown in Fig. 1[35], after mixing with anti-solvent rapidly, the solute concentration rose up to the saturation concentration (C^*) and reached to the critical nucleation concentration (C_n) where the precipitation process was triggered At this stage, the nuclei formed rapidly and grown by coagulation and condensation of solute until they reached to a critical value where they are stable. After nucleation and precipitation proceeding, the solute concentration fell down to the critical nucleation threshold (C_n), where new nucleation cannot be occurred any more[36]. While the growth of the existed nuclei still continued until the solute concentration fell to the saturation solubility (C^*)[37]. Finally, the formed nanoparticles would be stabilized with surfactants or aggregated without surfactants.

In order to obtain stable and ultrafine nanoparticle with a small distribution coefficient, it requires creating a higher nucleation rate but a negligible growth of nanoparticles. A higher degree of

supersaturation of solute in solution was demonstrated to result in the reducing system Gibbs free energy (ΔG_{cr}) of solution according to the Eq. (2), which leads to a higher nucleation rate (B) follows an Arrhenius relationship[35,38].

$$B = k_1 \exp\left(-\frac{\Delta G_{cr}}{KT}\right) \tag{2}$$

where k_1, K, T and ΔG_{cr} respectively represent a constant, i.e., the Boltzmann's constant, the temperature in Kelvin scale and the critical system Gibbs free energy for nucleation.

Nucleation and growth happened simultaneously throughout the particle formation and both compete for consuming the supersaturation of solute. If the nucleus growth dominates in the supersaturation, the final particles exhibit a large particle size and broad size distribution[39]. Therefore, it is very crucial to enhance the solute nucleation and inhibit nucleus growth in the particle formation process. As shown in Fig. 2, it showed that two dominating time scales related to the process of nanoparticle formation named mixing time (τ_{mix}) and particle formation time (τ_{flash})[27,40], where τ_{flash} is
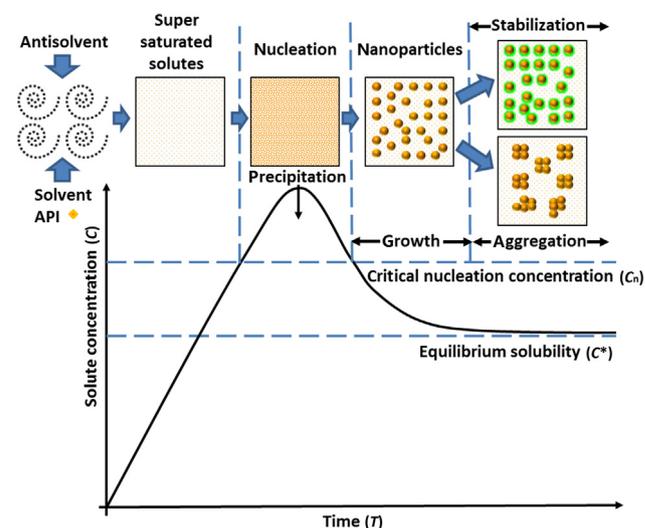

Figure 1 La Mer model[35] and schematic diagram of the nanoparticle forming process during the FNP.
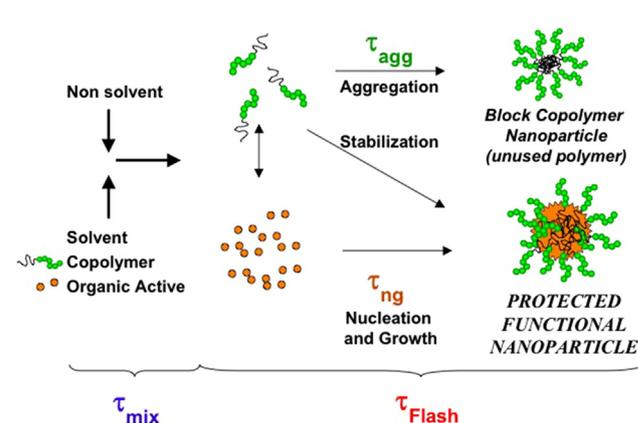

Figure 2 Schematic representation of the process of FNP of organic actives and block copolymers (Reproduced from Ref. 27 with permission. Copyright © 2003 CSIRO Publishing.).
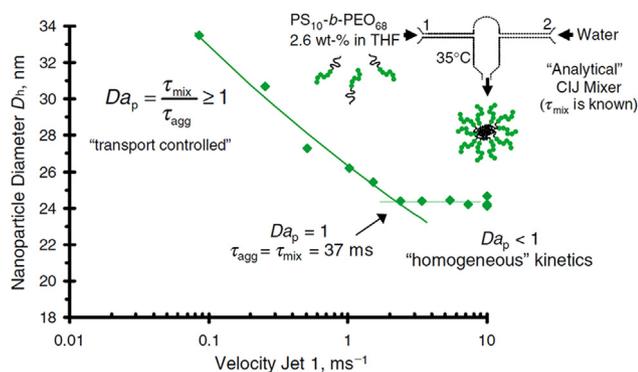
Figure 3 The relationship between the mixing rate and nanoparticle size in a CIJM (Reproduced from Ref. 27 with permission. Copyright © 2003 CSIRO Publishing.).

composed of drug nucleation and growth time (τ_{ng}) as well as the aggregation time of the block copolymer (τ_{agg}).

These time scales are very important to the particle formation process and controlled by mixing. The ratio of τ_{mix} to τ_{flash} corresponds to a dimensionless Damkohler number for precipitation (Da_p) in Eq. (3):

$$Da_p = \frac{\tau_{mix}}{\tau_{flash}} \qquad (3)$$

As shown in Fig. 3, when $Da_p < 1$, the mix process occur in a shorter period than the time required for the nucleation and growth phase. In this situation, supersaturation is attained rapidly and metastable state (*i.e.* the concentration between the saturation concentration and critical nucleation concentration of solute) is crossed quickly. Nucleation takes place rapidly and dominates in the FNP process. It will generate to a mass of drug nuclei and preparation of small and uniform drug nanoparticles. Otherwise, when $Da_p > 1$, the mixing time (τ_{mix}) of fluids is longer compared to the time of precipitation process (τ_{flash}) and the critical nucleation concentration of solute is reached slowly. The metastable state of the solute is crossed very slowly. It will lead to the dominance of nucleus growth and particle size increasing. Therefore, it is necessary to increase the mixing rate and decrease the mix time of solvent and anti-solvent in the FNP. Microfluidic mixer devices with specialized mixing geometries, such as CIJM or MIVM, could offer rapid mixing in the order of milliseconds to microseconds by shortening the diffusion distance between solvent and anti-solvent due to their microscale.

2.2. Parameters to be considered

The crucial properties of drug nanoparticles, such as particle size, polydispersity, zeta potential, morphology, purity and stability, are primarily associated with the rate, magnitude and uniformity of supersaturation of solute created in the mixing system. While the properties or parameters of drugs, solvent, anti-solvent, stabilizers and temperature have a great influence on the nature of the formed nanoparticles described below.

2.2.1. Drugs

FNP method is commonly used to fabricate a large number of hydrophobic drug nanoparticles. For successful encapsulation of lipophilic drug into nanocarriers, the nucleation and growth of drug molecule should generate before the formation of the final nanoparticles. So this will require drug molecule do not dissolve in aqueous solution easily. When selecting drugs with suitable solubility, the log P or calculated log P (Clog P) can be considered as a key indicator of hydrophobicity. As the log P is the negative logarithm of the partition coefficient of the dissolved drug molecule between *n*-octanol and water, a higher log P suggests a more hydrophobic drug. Pustulka et al.[41] suggested that nanoparticles of small molecule drug with Clog P less than 6 produced by FNP were unstable and underwent rapid Ostwald ripening. Zhu's study further suggested that when Clog $P > 12$, drug nanoparticles were stable; when $2 < $ Clog $P < 9$, drug nanoparticles would occur fast Ostwald ripening and recrystallization; when Clog $P < 2$, the drug was too soluble to form the nanoparticles by FNP [42]. In general, the higher the log P of the drug molecule, the better the physical stability of the formed drug nanoparticles. Therefore, the highly hydrophobic APIs including β-carotene[43–45], curcumin[46,47], cyclosporine A[48,49], doxorubicin[50,51] and itraconazole[52] were commonly used as model drugs in FNP reports. Moreover, some prodrugs with higher hydrophobicity than parent drug have been synthesized to facilitate encapsulation and/or improve nanoparticle stability[41,42,53,54]. However, the hydrophobicity is not the only parameter of the drug which influenced the physical stability of nanoparticles, other properties, like ionization and crystallinity of drug, also should also be considered[55,56].

In addition, the drug concentration in solvent is also important for the fabrication of drug nanoparticle by FNP. The drug concentration in solvent determined the degree of supersaturation created in the mixing process. A higher drug concentration would create a higher supersaturation level and nucleation rate, resulting in smaller particle size. Zhang et al.[57] found increasing drug concentration from 20 to 60 mg/mL favored to decrease particle size from 410 to 240 nm. On the other hand, the drug concentration at 80 mg/mL, the drug particles tend to aggregate and increase the particle size. Zhang et al.[58] investigate the effect of the cefuroxime axetil (CFA) concentration on the particle size without stabilizers. They found the particle size increased from 300 to 800 nm with the CFA concentration in acetone increasing from 60 to 120 mg/mL. Although a high drug concentration leads to a higher supersaturation that increases the nucleation rate, at the same time, a large number of nuclei also increases the viscosity and reduce the diffusion which leads the particle aggregation[59]. In order to obtain the ultrafine drug nanoparticles, we need to screen the optimal drug concentration with balanced the nucleation rate and particle growth kinetics.

2.2.2. Solvent and anti-solvent

In general, the organic solvent will be composed by one or more polar organic solvents such as tetrahydrofuran (THF), acetonitrile, dimethyl sulfoxide (DMSO), acetone, dimethyl formamide (DMF) and ethanol, which should be freely miscible with anti-solvent. The anti-solvent usually refers to water or aqueous buffer solution. Generally, the ideal organic solvent should have the highest capacity to dissolve the drugs and other hydrophobic excipients, such as polymers, lipids or surfactants, to ensure high supersaturation degree for precipitation. FNP is based on high supersaturation condition of drug molecule to trigger nucleation and growth of nanoparticles under controlled solvent/anti-solvent mixing conditions. Firstly, the various solvent/anti-solvent ratios impose different level of supersaturation for controlling

nanoparticle growth. For FNP, a low volume ratio of solvent/anti-solvent will create a high supersaturation level and help to increase the nucleation rate of drug nanoparticles. While the high volume ratio of solvent/anti-solvent increases the drug solubility in the mixed solution which creates lower supersaturation level and confines the drug nucleation induction. Second, the mixing rates of solvent and anti-solvent which is relevant to τ_{mix} influence the nucleation and growth of solute. The detained elaboration has been shown in Section 2.1. Since the formed nanoparticles were dispersed in aqueous and organic solvent mixtures, the organic solvent needs to be removed from the system. Meanwhile, the organic solvent in the mixed solution will enhance Ostwald ripening due to that organic solvent will enhance the intrinsic solubility of drugs. Therefore, the removal of the organic solvent from the drug nanoparticle formulation may reduce Ostwald ripening and thus improve physical stability[60]. Solvents with high boiling points such as DMSO and DMF are removed by dialysis, while the low boiling point solvents, like THF, acetone and ethanol, can be removed by vacuum evaporation. In addition, the FNP generally combined with freeze-drying[47,61] or spray-drying[48,62,63] to remove the solvent and stabilize the drug nanoparticles for long-term storage.

2.2.3.   Stabilizers

For drug nanoparticles prepared by FNP, the stabilizers have great influence on their formed particle size and long-term stability during storage. Reduction of the particles to nanometer scale greatly enhanced their surface area as well as the excessive interfacial energy. It is thermodynamically unstable due to agglomeration to large particles will happen to minimize the excessive interfacial energy. Many stabilizers were used to encapsulate drugs or protect drug nanoparticles from growing and agglomeration, hence stabilize the drug nanoparticles. The stabilizers adsorbed on the nanoparticles surface during the FNP process can decrease particle size significantly by reducing the interfacial energy at solid-liquid interface and increasing the nucleation rate[40,64]. On the other hand, it also can provide a long-term stability by limiting the Ostwald ripening[65], crystal form transformation[66,67] and nanoparticle agglomeration[68,69].

The selection of the stabilizer and its concentration is crucial to stabilize the drug nanoparticles with smaller size. The types of stabilizer used in FNP could be non-ionic polymer (HPMC, PMMA, HPC, HPMCAS, CMCAB), ionic polymer (NaCMC, NaAlg, Chitosan, PEI, PAH, Chitosan, PSS), linear polymer (PVP, PVA, PEG, PAA), hydrophobic polymer (PLGA, PLC, PLA), amphiphilic copolymer (poloxamer, PEG-PCL, PEG-PLA, PEG-PS, PEG-PLGA), surfactant of ionic type (SDS, CTACl, sodium cholic acid, sodium deoxycholic acid) or non-ionic type (Tween, Span, TPGS, lecithin, DSPE-PEG, Cremophor EL). The affinity of different stabilizers on drug surface determines their adsorption kinetics. The higher affinity of stabilizer–drug is, the faster stabilizer adsorbs on the drug surface, and hence the smaller drug nanoparticles are acquired[70]. The affinity strength of stabilizer–drug depends on the properties of the stabilizer and drug. For instance, stabilizers with higher hydrophobicity and higher H-bonding capacity (with more hydroxyl and carboxylic group) often had better affinity to the particle surface[71]. Dalvi and Dave[39] found that HPMC (more hydrophobic and more hydroxyl for H-bonding) is more effective than PVP (less hydrophobic, less H-bonding) for stabilizing griseofulvin nanoparticles. In a simple principle, the affinity of stabilizer–

drug is directly proportional to the strength of stabilizer–drug interaction and inversely proportional to the strength of stabilizer–solution (liquid phase) interactions[72,73]. The atomic force microscopy (AFM) can also be used to predict the affinity of stabilizer–drug in aiding stabilizer selection[74].

In addition to the affinity of stabilizer to drug surface, steric stabilization and electrostatic repulsion also play a significant role in the drug nanoparticle stabilization. For steric stabilization, the amphiphilic polymer and non-ionic polymer are appropriate for stabilizing nanoparticles prepared by FNP due to their large hydrophobic and hydrophilic block. The hydrophobic block can provide strong van der Waals force with the lipophilic drugs, resulting in high adsorption and encapsulating drug molecule. The hydrophilic block distribute on the particle surface, providing steric stabilization and preventing aggregation of drug nanoparticles. Thus, the size and molecular weight of polymer are important for drug nanoparticle stabilization. Hydrophilic PEG containing amphiphilic polymers are popular as PEG prolongs nanoparticle circulation in vivo[75]. Hydrophobic blocks, such as PLGA, PLA and PCL are commonly used as core materials[42–44]. It has been found that the incorporation of some hydrophobic molecule as co-stabilizer such as cholesterol could facilitate the rearrangement of amphiphilic stabilizer toward a micelle-like structure, and thus prolonging the particle stability[52]. For electrostatic stabilization, the charged ionic polymer and surfactant can offer repulsive force between particles due to similar charges on particle surface. The β-carotene and paclitaxel were stabilized with polyelectrolytes, such as ε-PL, PEI, chitosan and NaAlg, to form the polyelectrolyte complexes by FNP[45,76]. Ionic stabilizers formed an electric double layer around hydrophobic drug particles to prevent agglomeration. Actually, the surfactants often combined with polymeric stabilizers to enhance the drug nanoparticle stabilization through synergistic effect. The studies found that the combination of HPMC with SDS was more effective for drug nanoparticle stabilization than HPMC alone or HPMC–Tween 80 combination[38,66] because the ionic surfactant SDS offered the electrostatic repulsion and HPMC offered the steric protection to the drug particles. On the other hand, the surface properties of the nanoparticles were also largely determined by the stabilizers, such as zeta potential, morphology[69], long circulation[77], and cellular uptake ability[78].

The optimal concentration of the stabilizer for smaller particle size and better stabilization often depends on its water solubility and molecular structure. For surfactant, increasing its concentration is favor to the faster adsorption on solid liquid interface due to the higher concentration gradient and thus results in smaller drug nanoparticles[79]. For polymer, lower concentration is required due to its low critical flocculation concentration (CFC) and large molecular weight. An increasing polymer concentration generally increased drug particle size and encapsulation efficiency[80,81]. Because the high concentration polymer with large molecular weight significantly increased the viscosity of solvent which impeded the drug diffusion and result in large particle size[82]. For instance, Guhagarkar et al.[79] found the particle size decreased from 1000 to 300 nm with the PVA increasing from 0.1% to 0.5%. When further increased the PVA concentration to 4%, the particle size increased due to the increased viscosity. Using Pluronic F68 and Tween 80 as surfactants, the particle size decreased with the concentration increasing from 0.1% to 4%.

2.2.4.   Temperature

Temperature also plays an important role in particle size and particle size distribution by controlling solubility, supersaturation, nucleation rate and process kinetics during the FNP process. Usually, the FNP was operated at room temperature. Kim and Tan[83] evaluated the effect of precipitation temperature on the particle size in FNP. The nanoparticles decreased from 560 to 232 nm with the precipitation temperature reducing from 54 to 25 °C. As the above, a decrease in temperature reduces the equilibrium solubility and increases the level of supersaturation which increases the nucleation rate, decelerates the coagulation rate and reduces Ostwald ripening at a lower temperature. Thus, some researchers operated at low temperature to fabricate the smaller drug nanoparticles with narrow distribution, such as at 4 °C and in ice-bath[84,85].

3.   Mixing devices

3.1.   Confined Impingement Jets Mixer (CIJM)

The confined impinging jets were widely used for production of nanoparticles of water insoluble drugs *via* FNP. As shown in Fig. 4, the CIJM consists of a syringe pump and a mixing chamber with two opposing liner jets. The two fluid streams in opposing liner jets were drove to collide at high velocity by syringe pump to reduce the scale of segregation between the micro-volume liquid streams in the mixing chamber. Actually, Johnson and Prud'homme first evaluated FNP in detail using a CIJM in 2003[26]. In confined impinging jets mixer, the different jets diameters, chamber size, geometry and outlet configurations affect the process performance of the mixer[26,86,87]. They fully characterized the micro-mixing in impinging jets that could predict the mixing performance, reaction selectivity, and scale-up criteria.

Many researchers have used this CIJM to prepare various drug nanoparticles summarized in Table 1. They were mainly applied in the preparation of drug polymeric micelles[42–44,46,47,50], polymeric nanoparticles[88–90] and solid lipid nanoparticle[48,49,91] by nanoprecipitation methods. The high mixing efficiency and uniformity *via* CIJM were helpful in creating high supersaturation and high nucleation rates, which generated small and uniform nanoparticles with higher drug encapsulation efficiency (DEE) and drug loading capacity (DLC). For the CIJM, the flow rate of liquid jets is an important process parameter. As mentioned in the principle of FNP, the increasing in the flow rates of the opposite liquid jets will contribute to the higher supersaturation levels and thus higher nucleation rates, which generate smaller and uniform nanoparticles. Turino et al.[88] prepared PCL and PLGA nanoparticles with different particle size at different flow rates from 40 to 120 mL/min. Their study showed the higher velocity of the two opposite streams, the smaller nanoparticles obtained. The mixing in the CIJM can be as fast as milliseconds, but the CIJM is limited by the requirement of near equal flow rate of the opposed streams. So the volume ratio of organic solvent and anti-solvent (water) is 1:1. Because the presence of the organic solvent which is half volume of the mixed solution will significantly increase the drug solubility and limit the highest achievable supersaturation[55], the device of CIJM for the preparation of drugs nanoparticles formulations always equipped with a subsequent dilution process. Han et al.[43]
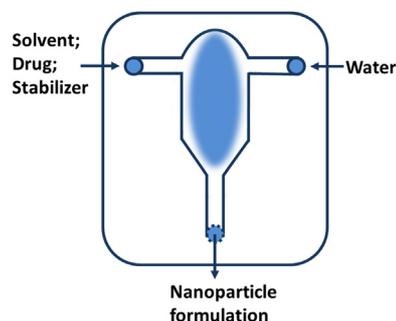

Figure 4   Schematics of confined imping jet mixer (CIJM).

prepared the *β*-carotene PEG-*b*-PLA nanoparticle (formulation volume: 5 mL) by the CIJM with the immediate dilution into 45 mL water at the ratio of 1:9. The resulting mean particle size was 55 nm and the formulation was stable. Nanoparticles prepared without dilution were highly unstable and grew to micron size within seconds. The dilution ratio after mixing in the CIJM also influenced the drug nanoparticle size and stability. As shown in Table 1, the dilution ratio (formulation volume *vs.* water volume) was generally from 1:9 to 2:1. So for CIJM with equal flow ratio of solvent to anti-solvent, immediate dilution with a large amount of anti-solvent (water) is essential to generate fine and stable nanoparticles. As list in Table 1, most the mass ratios of drug to stabilizer were 1:1 or less than 1. This maybe because too much amount of drug would increase the drug particle size and be adverse to the stability of drug particle. For CIJM, because the temperature control in the process was inconvenient, most of CIJM were operated under room temperature.

The particle size, zeta potential (ζ), polydispersity index (PDI) and stability of nanoparticle drugs produced by CIJM were also summarized in Table 1. The size of nanoparticle drugs was all almost in the nanoscale (< 1000 nm). The particle size distributed uniformly, and polydispersity index (PDI) was below 0.3. The zeta potential (ζ) of nanoparticle drugs was almost electrically negative or neutral. The Zeta potential (ζ) was primarily determined by the polymer and stabilizer of nanoparticle drugs. For the poorly water-soluble nanoparticle drugs prepared by nanoprecipitation, the drug encapsulation efficiency (DEE) could be more than 90%[46,92]. The high EE is due to the drugs have limited solubility in water, and thus most of them are encapsulated immediately in the nanoparticles upon FNP. Except the drug properties, the drug encapsulation efficiency (DEE) and drug loading capacity (DLC) also related to the formulation prescription and process, such as the solvent, flow rate, dilute ratio, stabilizer, especially the drug to stabilizer ratio. Most of the drug nanoparticles have low crystallinity, which could be due to the rapid precipitation of drug molecule and the effect of polymers and stabilizers prevent the formation of long-range order of drug crystals during FNP processes. However, because the amorphous drugs were easily to recrystallize in water and thus increased the particle size the researchers usually combined the CIJM with freeze drying or spray drying to stabilize the nanoparticle drugs for storage. For example, Chow et al.[47] prepared the curcumin (CUR) PEG-PLA nanoparticles using the CIJM. They found that the CUR nanoparticles were unstable even after proper optimization due to the nanoparticle aggregation and CUR recrystallization. After freeze drying with cyclodextrins derivatives Kleptose, the CUR nanoparticles had a good long-term storage stability (>1 year). Chiou et al.[48]

Table 1 Application of CIJM in drug nanoparticles fabrication.

API (log P)[a]	Solvent (S)	Flow rate (S/W flow ratio)	Dilute ratio[b]	Stabilizer	API/Stabilizer mass ratio	Mean size (nm)	Zeta (mV)	PDI	Stability[c]	Ref.
β-Carotene (15.232)	THF	30 mL/min (1:1)	1:9	PEG-PLA	1:1	55	n/a	n/a	n/a[d]	43
		72 mL/min (1:1)	1:4	PEG-PCL; PEG-PS	2:1–2:9	70–130	n/a	n/a	n/a	44
Curcumin (2.517)	Acetone/DMF/ THF	n/a (1:1)	1:9	PEG-PLA	1:1	70–150	−0.715	0.05–0.2	2 h	46
	Acetone	30 mL/min (1:1)	1:9	PEG-PLA; PVP	1:1	< 100	0.11	n/a	5 day	47
Doxorubicin (1.27)	Acetone or THF	40 to 120 mL/min (1:1–1:8)	n/a	P(MePEGCA-co-HDCA)	1:20–1:5	80–300	−20 to −50	n/a	n/a	50
Paclitaxel (4.73)	THF	72 mL/min (1:1)	1:9	PEG-PLGA	1:1	122	n/a	n/a	90 min	42
Paclitaxel prodrug (18.36)					1:1	86			8 day	
Florfenicol (2.84)	Acetone	40, 80 or 120 mL/min (1:1)	2:1	PCL	1:12–5:6	230–300	−32 to −40	< 0.1	n/a	88
				PLGA	1:12–5:6	70–105	−15 to −25	< 0.2		
Melatonin (1.34)	Acetone	5 to 120 mL/min (1:1)	2:1	PCL	0.18–6	250–400	−17 mV	n/a	n/a	89
Menthol (3.216)	Acetone/ACN/ THF	5 to 120 mL/min (1:1)	0.24–2	PCL	0.76–2	200–500	−20 to −45	0.05–0.3	n/a	90
Cyclosporine A (3.0)	Ethanol	120 mL/min (1:1)	1:5	Soy lecithin; lactose	10:1.025	180–700	n/a	n/a	n/a	48
		40:120 mL/min (1:3)	4:5	Lecithin; dextrose monohydrate	0.7:1.8	260				49
Clofazimine (7.66)	Acetone/THF	12 mL/min (1:1)	1:4	HPMCAS	n/a	90	−28.7	0.24	n/a	91
				Lecithin	n/a	170	−52.3	0.16		

[a]The data of Log P was experimental Log P from Scifinder database.
[b]The volume ratio of formulation volume *vs.* water volume.
[c]The minimum stability time at room temperature, if no otherwise specified.
[d]n/a, the data was not mentioned or determined in the paper.

used CIJM to produce cyclosporine (CsA) nanoparticles with lecithin and lactose, followed by spray drying to produce dry powder for inhalation.

3.2. Multi-Inlet Vortex Mixer (MIVM)

To overcome the limitation of the CIJM yet keep its ability of rapid mixing, scalability, and ease of operation, Prud'homme and coworkers[29] further developed MIVM (Fig. 5), which is also commonly used for FNP. In this device, the mixing chamber is connected to four inlets and the liquid streams were drove to collide at an angle with high velocity by syringe pumps, thus the mixing adopts vortex principle. Since each stream contributes independently to the micromixing process in the mixing chamber, the MIVM can be applied to various solvent ratios and materials. It can freely adjust flow rate of solution and anti-solvent in mixer to achieve different levels of supersaturation, thus to manipulate the nucleation and growth time scale. The high-efficiency and rapid mixing rates of solution and anti-solvent in MIVM ensured that the mixing time is shorter than nucleation and growth time of nanoparticles. Because of the flexibility to adjust the solvent ratios and materials by varying the content and flow velocity of incoming streams, MIVM has stronger function and wider application than CIJM in the preparation of poorly water-soluble drug nanoparticles as shown in Table 2. The MIVM was mainly applied in the preparation of drug polymeric micelles[34,46,61], polymeric nanoparticles[96,97,108], polyelectrolyte complex[34,45], nanocrystal drug[102,107] and solid lipid nanoparticle[62,104,106].

Similar to CIJM, the flow rate of liquid streams is also an important process parameter for MIVM. In addition to the flow rate, MIVM has a higher flexibility for stream arrangement due to multiple inlets, such as solvent/solvent/water/water (S/S/W/W)[34,45], solvent/water/solvent/water (S/W/S/W)[114] and solvent/water/water/water (S/W/W/W)[34,46]. The volume ratio of organic solvent to water solution could be varied from 1:41 to 1:1. The most commonly used volume ratio of organic solvent to water was 1:9 or 1:19. Therefore, through the manipulation of flow rate and composition of the liquid streams, MIVM is more flexible to obtain different levels of supersaturation to control particle size. But different from CIJM, MIVM provides the final drug formulation with very low organic solvent concentration and thus reduces the Ostwald ripening of resulting drug nanoparticles. MIVM can produce stable and small drug nanoparticles without further dilution process. The mass ratios of drug to stabilizer were also mostly 1:1 or less than 1 as list in Table 2. The particle size, zeta potential (ζ), polydispersity index (PDI) and stability of nanoparticle drugs produced by MIVM were summarized in Table 2. The size of drug nanoparticles was all almost in the nanoscale (< 1000 nm). The particle size distributed uniformly, and polydispersity index (PDI) were all below 0.3. The Zeta potential (ζ) was primarily determined by the polymer or stabilizer of drug nanoparticles. For instance, the β-carotene polyelectrolyte complexes were electropositive. Due to they were stabilized by electrostatic interaction with cationic polymer, such as ε-PL, PEI and chitosan.

Same as the drug nanoparticles prepared by CIJM, most of the drug nanoparticles prepared by MIVM were amorphous[62,93,99]. For the poorly water-soluble drug nanoparticles fabricated by FNP, compact and ordered crystalline structure could not be generated due to insufficient time available for crystals growth. The highly disordered amorphous nanoparticles with high free energy could increase the drug
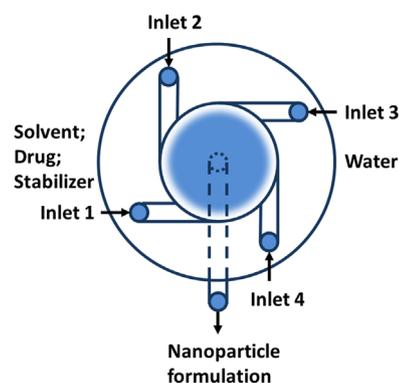

Figure 5 schematics of multi-inlet vortex mixer (MIVM).

dissolution rate and water solubility, which in favor to higher bioavailability of poorly water-soluble drugs. However it will also bring problem for drug nanoparticles due to its thermodynamic instability. The metastable amorphous drug nanoparticles tend to convert to its stable crystal form during storage as mentioned in Section 3.1. The transformation of drug crystalline form is a physical process referred to phase change and equilibrium, which mainly included the mechanism of solid–solid phase transformation and solution-mediated phase transformation[115]. For drug nanoparticles fabricated by FNP, most of the crystalline transformations were the solution-mediated phase transformation in water. According to this mechanism[116,117], the metastable amorphous drug nanoparticles dissolved continually and a new more stable crystal form then nucleated and grew in water. The new formed drug crystal grew larger and larger until the amorphous drug nanoparticles dissolved completely. Because of the solubility of the metastable crystal is higher than that of the stable crystal, the difference of the solubility of the different crystal forms is the driving force of the crystalline transformation. Therefore, many studiers used suitable excipients[66,67] and combined with freeze-drying or spray-drying by removing water medium to stabilize the drug nanoparticles as amorphous[61–63,97,98,104–106,108,112].

3.3. Microfluidic mixer systems

Microfluidic mixer systems have been widely used in the fields of chemical synthesis, diagnosis, crystallization, combinatorial synthesis, nanoparticles synthesis, biochemical assays and high-throughput screening[118,119]. More recently, microfluidic mixer systems have been the powerful devices for nanoparticles preparation in microliter scale. As the name suggests, microfluidics refers to the fluid in networks of channels with micrometer scale, and the reaction volume is greatly reduced to microliters. Due to the micron-sized scale, microfluidics behavior differs from conventional flow theory. As suggested by the low Reynold's number in the microfluidic mixer, liquid flow patterns were deemed as laminar in parallel without turbulence[120,121]. Mixing occurred as a result of diffusion of molecules across the interface between solvent and anti-solvent fluids within microseconds as the schematics shown in Fig. 6. Microfluidic mixer systems maximized the mixing performance, leading to the highest mixing efficiency and homogeneous reaction environment of the solute solution under continuous flow condition. In addition, the microfluidic mixers possess a high surface to volume ratio and consequently highly efficient heat transfer and

Table 2 Application of MIVM in nanoparticles fabrication.

API (log P)[a]	Solvent (S)	Flow rate of streams	S/W ratio[b]	Stabilizer	API/Stabilizer mass ratio	Size (nm)	Zeta (mV)	PDI	Stability[c]	Ref.
β-Carotene (15.232)	THF	S/S/W/W=13.3/13.3/120/120 (mL/min)	1:9	ε-PL	1:1	150–180	+50	n/a	1 week	45
				PEI	1:1	50–102	+15 to +70		5 week	
				Chitosan	1:1	55–100	+25 to +40		1 week	
		S/S/W/W=1:1:1:1–1:1:9:9	1:9–1:1	PEG-PS; PEG-PCL	1:1	50–250	n/a	n/a	n/a[d]	34
		S/S/W/W=1:1:10:10	1:10	PEG-PLGA	1:1	110–140	n/a	n/a	n/a	63
		S/W/W/W=12/12/48/48 (mL/min)	1:9	Dex-PLLA	1:1	177	n/a	0.165	n/a	92
		S/S/W/W=13.3/13.3/120/120 (mL/min)	1:9	PEG-PS; PEG-PLA; PEG-PCL	1:1	30–70	–20	n/a	n/a	93
				PEG-PLGA	1:1					42,93
		S/S/W/W=6/6/24/24–6/6/78/78 (mL/min)	1:13–1:4	PEG-PCL	1:100–1:1	< 210	n/a	0.12	n/a	94
		S/W/W/W=30/30/30/30–36/9/9/9 (mL/min)	1:3–1	PEG-PLA	1:20–1:1	28	n/a	0.1	n/a	95
Curcumin (2.517)	Acetone/DMF/THF	S/W/W/W=1:10:1:10	1:21	PEG-PLA	1:1	90–120	–0.132	0.1–0.3	2 h	46
	DMF	S/W/W/W=5/45/5/45 (mL/min)	1:19	PEG-PLA and PVP	1:1:1–1:1:0.8	< 80	–0.29	0.09	n/a	61
		S/W/W/W=10/90/10/90 (mL/min)	1:19	PLGA and PVP	1:1:0.8	50	n/a	0.11	n/a	96
	THF	S/W/W/W=6/6/54/54 (mL/min)	1:19	PLGA	1:1	50–250	–33.1	n/a	10 min	97,98
				PEG-PLA	1:1	120	–2.5		n/a	98
		S/W/W/W=3:10:10:10	1:10	CMCAB; PLGA	1:1	200	–35 to –41	0.2–0.25	n/a	99
		S/W/W/W=5.82/6.5/6.5/6.5 (mL/min)	3:10	CMCAB; PLGA	1:9–1:1	167–202	–35 to –48	0.2–0.25	n/a	100,101
	ethanol	S/W/W/W=11/11/99/99 (mL/min)	1:19	PVP	1:8	20	–8.21	0.37	1 month[e]	102
Curcumin SPIO (n/a)	DMF	S/W/W/W=5/45/5/45 (mL/min)	1:19	PEG-PLA	1:2	< 100	–0.4	0.14	n/a	103
Cyclosporine A (3.0)	Ethanol	S/S/W/W=30/30/30/30 (mL/min)	1:1	Lecithin and lactose	0.125:5:50	200–300	n/a	n/a	n/a	62,104,105
				TPGS	50:1	160	n/a	0.08	n/a	105
		S/S/W/W=20/20/30/30 (mL/min)	2:3	Lecithin and lactose	0.125:5:50	170	n/a	n/a	n/a	106
Paclitaxel prodrug (n/a)	THF	S/W/W/W=12/40/40/40 (mL/min)	1:10	PEG-PS; PEG-PLA;	1:1	50–110	n/a	n/a	n/a	54
		S/S/W/W=13.3/13.3/120/120 (mL/min)	n/a	PEG-PCL; PEG-PLGA	1:1	100	n/a	n/a	n/a	41
Ursolic acid (8.731)	Ethanol	S/W/W/W=2/2/10/10–8/8/40/40 (mL/min)	1:11	PVP K90 and SDS	3:5.5:5.5	100–300	–8 to –10	< 0.25	5 week	107
Nitric oxide (NO) prodrug (n/a)	THF	S/W/W/W=12/40/40/40 (mL/min)	1:10	PEG-PS	3:8.6	240	n/a	n/a	n/a	53
				PEG-PLA	3:8.6	225				
SR13668 (n/a)	THF	S/W/W/W=6/6/54/54 (mL/min)	1:19	PLGA	1:4–1:1	150	n/a	n/a	24 h	108
Doxorubicin (1.27)	DMF; acetone	S/W/W/W=10/90/10/90 (mL/min)	1:19	PEG-PLA and PVP	1:5–1:1	< 100	–0.25	0.15–0.3	30 day[e]	51
Cholesteryl bodipy (n/a)	THF	S/W/W/W=10/100/100/100 (mL/min)	1:30	PLA and Tween 80	0.01:10:30	196.0	–18.5	0.173	n/a	109
TIPS pentacene (15.385)	THF	S/W/W/W=9.99/33.3/33.3/33.3 (mL/min)	1:10	PEO-PDLLA	1:100-1:50	90–115	–14	0.28	n/a	110
Itraconazole (6.2)	DMF	S/W/W/W=11/11/99/99 (mL/min)	1:19	TPGS	1:1	91.1	–10	0.101	15 day[e]	52
				PEG-PLA	1:1	120	–20	n/a		
Ritonavir (4.9); Efavirenz (3.035)	THF	S/W/W/W=3:10:10:10	1:10	CMCAB; CAP Adp 0.33; CAP Adp 0.85; CA 320 S Seb	1:3	100–200	n/a	0.2	n/a	111
Clarithromycin (3.16)	THF	S/W/W/W	n/a	CMCAB	100:33	100	n/a	n/a	n/a	112
Schisanterin A (4.901)	Acetone	S/W/W/W=4/4/80/80 (mL/min)	1:41	PEG-PLGA and HPMC E3	4:4:5	70	–24.7	0.104	6 h	113
Clofazimine (7.66)	Acetone	S/W/W/W=12/12/36/36 (mL/min)	1:7	Zein and NaCas	2:2:1	240	–46.4	0.11	n/a	91

[a]The data of Log P was experimental Log P from Scifinder database.

[b]The volume ratio of solvent vs. anti-solvent (water).

[c]The minimum stability time at room temperature, if no otherwise specified.

[d]n/a means the data was not mentioned or determined in the paper.

[e]The minimum stability time at 4 °C.

temperature control, which is the special advantage over the regular mixer, such as CIJM and MIVM. Zhao et al.[120] prepared danazol nanoparticles *via* microfluidic mixer under the conditions of different anti-solvent temperatures, where the particle size prepared at 4 °C was apparently smaller than that obtained at 30 °C with more narrow particle size distribution.

With the further development of microscale mixers of nanoparticles fabrication, microfluidic mixer systems have evolved from simple channel to more functional and complex systems for better controlling of operating parameters. Meanwhile, "on-chip" micro-fabricated systems provided a wide range of designs, from two dimensional layouts to fully three dimensional and more complex structures allows for precise manipulation of hydrodynamics for efficient mixing and controlled addition of reagents at precise time intervals[30,122].

There are various variations of microfluidic mixers available for FNP of poorly water-soluble drugs as shown in Table 3, such as Y-shape microfluidic mixer[120,123–126], T-shape microfluidic mixer[127], Planar flow focusing mixer[128–132], Cross-shaped Planar flow focusing mixer[133–137] and other specific microfluidic mixers[122,138–143]. The microfluidic mixers have been used for high throughput screening and properties controlling of various drug nanoparticles by adjusting the parameters. These have been used for preparation of nanocrystals[120,123–128], polymeric micelles[129–132,141], polymeric nanoparticles[122,133,134,139,140], solid lipid nanoparticles[135,136], lipid−polymer nanoparticles[142,143], polyelectrolyte complex[138], even the liposomes[137]. In addition, they could be integrated with the on-line measurement systems on a single technology platform. For example, the microfluidic mixer chips were integrated with miniaturized dynamic light scattering (DLS) as a powerful tool for real time and micro-monitor of nanoparticle[144,145]. Many more complicated microfluidic mixers for special-purpose were described in previous reviews[20,30,31] and will not described in detail here. Microfluidic mixer systems process the great potential for industrial-scale production of drug nanoparticle formulation by extensive mixers in parallel[146]. There are three levels to scale-up the production of drug nanoparticles, including expanding arraying identical channels, multi-layers with channel arrays and integrated mixer devices in parallel[30]. Li et al.[147] developed a continuous generation of polymer particles in parallel multiple modular microfluidic (M^3) reactors, which could produce polymer micro-gel particles with polydispersity not exceeding 5% at a productivity of 50 g/h. Also, Nisisako and Torii[148] produced the

monodisperse emulsion droplets and particles using microfluidic large-scale integration on a chip. The production module comprised 128 cross-junctions arranged circularly on a 4 cm × 4 cm glass chip, which could be applied in the mass production of homogeneous monomer droplets. Therefore, the research and development of these scaled-up microfluidic mixer systems would greatly promote the industrialization of nanoparticle drug by FNP.

4. Summary and future perspectives

As described before, many different nanoparticle formulations of poorly water-soluble drug have been prepared by FNP using CIJM, MIVM and other microfluidic mixer systems, indicating that FNP devices are the promising techniques for nanoparticle fabrication. FNP by microfluidic mixer devices is a simple, rapid and scalable method capable of continuously preparing drug nanoparticles with controlled sizes within 1000 nm, narrow size distributions and tailored surface properties. These laboratory devices are very helpful in optimizing conditions in favor of nanoparticle production. In FNP, the key to prepare ultrafine drug nanoparticles is to create the rapid, uniform and high supersaturation of solute to drive high nucleation rates. Moreover, the properties or parameters of drugs, solvent, anti-solvent, stabilizers and temperature also have a great influence on the formation of nanoparticles. The continuous and controllable production of ultrafine nanoparticles with good repeatability by microfluidic mixer devices makes it potentially scalable easily from laboratory to industrial scales. In addition, the microfluidic mixer devices can be conducted in parallel in hundreds units to scale up with the same operating condition.

However, there are also many issues need to be addressed for the FNP by microfluidic mixer devices. The residual organic solvent in the drug nanoparticles or formulations will result in instability of nanoparticles by Ostwald ripening after particle formation. In addition, it may also cause the medication safety problems to patients due to the toxicity of the residual organic solvent. The drug nanoparticles made by FNP were mostly amorphous and less stable as compared to their crystalline counterpart during storage. Therefore, freeze drying or spray drying is desirable to remove solvent and store the nanoparticles as solid state to enhance their long term stability.
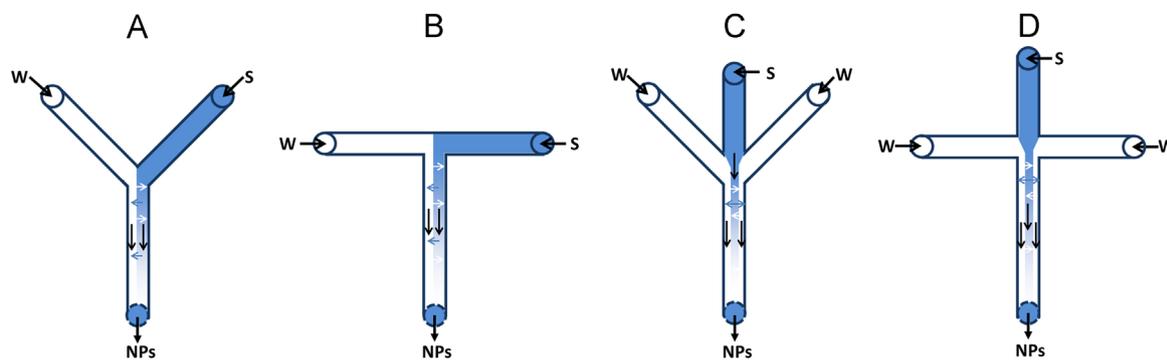

Figure 6 Schematics of Y-shape microfluidic mixer (A), T-shape microfluidic mixer (B), planar flow focusing mixer (C) and cross-shaped planar flow focusing mixer (D).

Table 3 Application of microfluidic mixers in nanoparticles fabrication.

Microfluidic device	API (log P)[a]	Solvent (S)	Stabilizer	API/Stabilizer mass ratio	Size (nm)	PDI	Formulation	Ref.
Y-shape microfluidic mixer	Danazol (4.20)	Ethanol	n/a[b]	n/a	364	n/a	Nanocrystals	120
	Hydrocortisone (1.43)		PVP; HPMC; SLS	2:1:1:0.25	80–450	0.21		123
			PVP; HPMC; Tween 80	5:2:5:1	300	0.18		124
	Cefuroxime axetil (0.11)	Acetone	n/a	n/a	350	n/a		125
	Atorvastatin calcium (n/a)	Methanol		n/a	210–760	n/a		126
T-shape microfluidic mixer	Curcumin (2.517)	Ethanol		n/a	190–450	n/a		127
Planar flow focusing mixer	Rubrene (13.731)	THF/EtOH: 30/70	CTACl	1:40	50–110	n/a		128
	n/a	DMSO	Pluronic F127	n/a	100–130	n/a	Polymeric micelles	129
	Mithramycin (1.29)			n/a	52–61	n/a		130
	Dexamethasone (1.83)			n/a	6–207	n/a		131
	β-Carotene (15.232)	THF		2.35	70	n/a		132
Cross-shaped planar flow focusing mixer	n/a	DMAc	Polybenzimidazole	n/a	70–120	n/a	Polymeric nanoparticles	133
		ACN	PEG-PLGA	n/a	10–50	n/a		134
		Acetone	Softisan 100; Pluronic F68	n/a	60–280	0.01–0.29	Solid lipid nanoparticles	135
		Ethanol		n/a	50–280	0.14–0.19		136
		Isopropyl alcohol	Lipid	n/a	100–300	n/a	Liposomes	137
2D flat chip	Doxorubicin (1.27)	DMF	PLGA	3:500	100–234	0.13	Polymeric nanoparticles	122
3D arc chip					< 100	0.13		
3D double spiral chip					< 100	0.06		
Rotating tube processor	Meloxicam (3.01)	n/a	PAH; PSS	n/a	< 100	0.015	Polyelectrolyte complex	138
Multi-inlet impact-jet micromixer	Ketoprofen (2.77)	THF	PMMA; Cremophor ELP	1:2:1	100	< 0.2	Polymer nanoparticles	139
High pressure interdigital multilamination micromixer (HPIMM)	n/a			n/a		< 0.3		140
3D flow focusing mixer	n/a	Acetonitrile	PEG-PLGA	n/a	30–230	n/a	Polymeric micelles	141
Tesla structure mixer			PLGA; Lipid; Lipid-PEG		40		Lipid−polymer nanoparticles	142
Microvortice mixer					30–170			143

[a]The data of Log P was experimental Log P from Scifinder database.
[b]The n/a means the data was not mentioned or determined in the paper.

Acknowledgement

References

1. Thorat AA, Dalvi SV. Liquid antisolvent precipitation and stabilization of nanoparticles of poorly water soluble drugs in aqueous suspensions: recent developments and future perspective. *Chem Eng J* 2012;**181-182**:1–34.
2. Dahan A, Miller JM, Hoffman A, Amidon GE, Amidon GL. The solubility–permeability interplay in using cyclodextrins as pharmaceutical solubilizers: mechanistic modeling and application to progesterone. *J Pharm Sci* 2010;**99**:2739–49.
3. Jain NK, Gupta U. Application of dendrimer–drug complexation in the enhancement of drug solubility and bioavailability. *Expert Opin Drug Metab Toxicol* 2008;**4**:1035–52.
4. Serajuddin AT. Salt formation to improve drug solubility. *Adv Drug Deliv Rev* 2007;**59**:603–16.
5. Stella VJ, Nti-Addae KW. Prodrug strategies to overcome poor water solubility. *Adv Drug Deliv Rev* 2007;**59**:677–94.
6. Vasconcelos T, Sarmento B, Costa P. Solid dispersions as strategy to improve oral bioavailability of poor water soluble drugs. *Drug Discov Today* 2007;**12**:1068–75.
7. Kalepu S, Nekkanti V. Insoluble drug delivery strategies: review of recent advances and business prospects. *Acta Pharm Sin B* 2015;**5**:442–53.
8. Shekhawat PB, Pokharkar VB. Understanding *peroral* absorption: regulatory aspects and contemporary approaches to tackling solubility and permeability hurdles. *Acta Pharm Sin B* 2017;**7**:260–80.
9. Zhou Y, Quan G, Wu Q, Zhang X, Niu B, Wu B, et al. Mesoporous silica nanoparticles for drug and gene delivery. *Acta Pharm Sin B* 2018;**8**:165–77.
10. Hu J, Johnston KP, Williams III RO. Nanoparticle engineering processes for enhancing the dissolution rates of poorly water soluble drugs. *Drug Dev Ind Pharm* 2004;**30**:233–45.
11. Xu Y, Liu X, Lian R, Zheng S, Yin Z, Lu Y, et al. Enhanced dissolution and oral bioavailability of aripiprazole nanosuspensions prepared by nanoprecipitation/homogenization based on acid-base neutralization. *Int J Pharm* 2012;**438**:287–95.
12. Chen C, Wang L, Cao F, Miao X, Chen T, Chang Q, et al. Formulation of 20(*S*)-protopanaxadiol nanocrystals to improve oral bioavailability and brain delivery. *Int J Pharm* 2016;**497**:239–47.
13. Zhang L, Gu FX, Chan JM, Wang AZ, Langer RS, Farokhzad OC. Nanoparticles in medicine: therapeutic applications and developments. *Clin Pharmacol Ther* 2008;**83**:761–9.
14. Mosqueira VC, Legrand P, Morgat JL, Vert M, Mysiakine E, Gref R, et al. Biodistribution of long-circulating peg-grafted nanocapsules in mice: effects of PEG chain length and density. *Pharm Res* 2001;**18**:1411–9.
15. Ahire E, Thakkar S, Darshanwad M, Misra M. Parenteral nanosuspensions: a brief review from solubility enhancement to more novel and specific applications. *Acta Pharm Sin B* 2018;**8**:733–55.
16. Keck CM, Müller RH. Drug nanocrystals of poorly soluble drugs produced by high pressure homogenisation. *Eur J Pharm Biopharm* 2006;**62**:3–16.
17. Müller RH, Möschwitzer J, Bushrab FN. Manufacturing of nanoparticles by milling and homogenization techniques. In: Gupta RB, Kompella UB, editors. *Nanoparticle technology for drug delivery*. New York: CRC Press; 2006. p. 45–76.
18. Shah P. Use of nanotechnologies for drug delivery. *MRS Bull* 2006;**31**:894–9.
19. Saad WS, Prud'homme RK. Principles of nanoparticle formation by flash nanoprecipitation. *Nano Today* 2016;**11**:212–27.
20. Ding S, Anton N, Vandamme TF, Serra CA. Microfluidic nanoprecipitation systems for preparing pure drug or polymeric drug loaded nanoparticles: an overview. *Expert Opin Drug Del* 2016;**13**:1447–60.
21. Astete CE, Kumar CS, Sabliov CM. Size control of poly(D,L-lactide-*co*-glycolide) and poly(D,L-lactide-*co*-glycolide)-magnetite nanoparticles synthesized by emulsion evaporation technique. *Colloid Surf A* 2007;**299**:209–16.
22. Allémann E, Leroux JC, Gurny R, Doelker E. *In vitro* extended-release properties of drug-loaded poly(DL-lactic acid) nanoparticles produced by a salting-out procedure. *Pharm Res* 1993;**10**:1732–7.
23. Jung J, Perrut M. Particle design using supercritical fluids: literature and patent survey. *J Supercrit Fluids* 2001;**20**:179–219.
24. Reverchon E. Supercritical antisolvent precipitation of micro- and nano-particles. *J Supercrit Fluids* 1999;**15**:1–21.
25. Kwon HY, Lee JY, Choi SW, Jang YS, Kim JH. Preparation of PLGA nanoparticles containing estrogen by emulsification–diffusion method. *Colloid Surf A* 2001;**182**:123–30.
26. Johnson BK, Prud'homme RK. Chemical processing and micromixing in confined impinging jets. *AIChE J* 2003;**49**:2264–82.
27. Johnson BK, Prud'homme RK. Flash nanoprecipitation of organic actives and block copolymers using a confined impinging jets mixer. *Aust J Chem* 2003;**56**:1021–4.
28. Johnson BK, Prud'homme RK. Mechanism for rapid self-assembly of block copolymer nanoparticles. *Phys Rev Lett* 2003;**91**:118302.
29. Liu Y, Cheng C, Liu Y, Prud'homme RK, Fox RO. Mixing in a multi-inlet vortex mixer (MIVM) for flash nano-precipitation. *Chem Eng Sci* 2008;**63**:2829–42.
30. Capretto L, Carugo D, Mazzitelli S, Nastruzzi C, Zhang X. Microfluidic and lab-on-a-chip preparation routes for organic nanoparticles and vesicular systems for nanomedicine applications. *Adv Drug Deliv Rev* 2013;**65**:1496–532.
31. Zhao CX, He L, Qiao SZ, Middelberg AP. Nanoparticle synthesis in microreactors. *Chem Eng Sci* 2011;**66**:1463–79.
32. Horn D, Rieger J. Organic nanoparticles in the aqueous phase—theory, experiment, and use. *Angew Chem Int Ed Engl* 2001;**40**:4331–61.
33. Söhnel O, Garside J. *Precipitation: basic principles and industrial applications*. Oxford: Butterworth-Heinemann; 1992.
34. Shen H, Hong S, Prud'homme RK, Liu Y. Self-assembling process of flash nanoprecipitation in a multi-inlet vortex mixer to produce drug-loaded polymeric nanoparticles. *J Nanopart Res* 2011;**13**:4109–20.
35. LaMer VK, Dinegar RH. Theory, production and mechanism of formation of monodispersed hydrosols. *J Am Chem Soc* 1950;**72**:4847–54.
36. D'Addio SM, Prud'homme RK. Controlling drug nanoparticle formation by rapid precipitation. *Adv Drug Deliv Rev* 2011;**63**:417–26.
37. Dirksen JA, Ring TA. Fundamentals of crystallization: kinetic effects on particle size distributions and morphology. *Chem Eng Sci* 1991;**46**:2389–427.
38. Mullin JW. In: *Crystallisation*. 2nd ed. London: CRC Press; 1972.
39. Dalvi SV, Dave RN. Controlling particle size of a poorly water-soluble drug using ultrasound and stabilizers in antisolvent precipitation. *Ind Eng Chem Res* 2009;**48**:7581–93.
40. Matteucci ME, Hotze MA, Johnston KP, Williams III RO. Drug nanoparticles by antisolvent precipitation: mixing energy *versus* surfactant stabilization. *Langmuir* 2006;**22**:8951–9.
41. Pustulka KM, Wohl AR, Lee HS, Michel AR, Han J, Hoye TR, et al. Flash nanoprecipitation: particle structure and stability. *Mol Pharm* 2013;**10**:4367–77.
42. Zhu Z. Flash nanoprecipitation: prediction and enhancement of particle stability *via* drug structure. *Mol Pharm* 2014;**11**:776–86.
43. Han J, Zhu Z, Qian H, Wohl AR, Beaman CJ, Hoye TR, et al. A simple confined impingement jets mixer for flash nanoprecipitation. *J Pharm Sci* 2012;**101**:4018–23.
44. Zhu Z, Anacker JL, Ji S, Hoye TR, Macosko CW, Prud'homme RK. Formation of block copolymer-protected nanoparticles *via* reactive impingement mixing. *Langmuir* 2007;**23**:10499–504.

45. Zhu Z, Margulis-Goshen K, Magdassi S, Talmon Y, Macosko CW. Polyelectrolyte stabilized drug nanoparticles *via* flash nanoprecipitation: a model study with *β*-carotene. *J Pharm Sci* 2010;**99**:4295–306.

46. Chow SF, Sun CC, Chow AH. Assessment of the relative performance of a confined impinging jets mixer and a multi-inlet vortex mixer for curcumin nanoparticle production. *Eur J Pharm Biopharm* 2014;**88**:462–71.

47. Chow SF, Wan KY, Cheng KK, Wong KW, Sun C, Baum L, et al. Development of highly stabilized curcumin nanoparticles by flash nanoprecipitation and lyophilization. *Eur J Pharm Biopharm* 2015;**94**:436–49.

48. Chiou H, Chan HK, Heng D, Prud'homme RK, Raper JA. A novel production method for inhalable cyclosporine a powders by confined liquid impinging jet precipitation. *J Aerosol Sci* 2008;**39**:500–9.

49. Chiou H, Chan HK, Prud'homme RK, Raper JA. Evaluation on the use of confined liquid impinging jets for the synthesis of nanodrug particles. *Drug Dev Ind Pharm* 2008;**34**:59–64.

50. Lince F, Bolognesi S, Stella B, Marchisio DL, Dosio F. Preparation of polymer nanoparticles loaded with doxorubicin for controlled drug delivery. *Chem Eng Res Des* 2011;**89**:2410–9.

51. Tam YT, To KK, Chow AH. Fabrication of doxorubicin nanoparticles by controlled antisolvent precipitation for enhanced intracellular delivery. *Colloid Surf B* 2016;**139**:249–58.

52. Wan KY, Wong KW, Chow AH, Chow SF. Impact of molecular rearrangement of amphiphilic stabilizers on physical stability of itraconazole nanoparticles prepared by flash nanoprecipitation. *Int J Pharm* 2018;**542**:221–31.

53. Kumar V, Hong SY, Maciag AE, Saavedra JE, Adamson DH, Prud'homme RK, et al. Stabilization of the nitric oxide (NO) prodrugs and anticancer leads, PABA/NO and double JS-K, through incorporation into PEG-protected nanoparticles. *Mol Pharm* 2010;**7**:291–8.

54. D'Addio SM, Saad W, Ansell SM, Squiers JJ, Adamson DH, Herrera-Alonso M, et al. Effects of block copolymer properties on nanocarrier protection from *in vivo* clearance. *J Controlled Release* 2012;**162**:208–17.

55. Liu Y, Kathan K, Saad W, Prud'homme RK. Ostwald ripening of *β*-carotene nanoparticles. *Phys Rev Lett* 2007;**98**:036102.

56. Tang C, Prud'homme RK. Targeted theragnostic nanoparticles *via* flash nanoprecipitation: principles of material selection. In: Vauthier C, Ponchel G, editors. *Polymer nanoparticles for nanomedicines.* Cham: Springer; 2016. p. 55–85.

57. Zhang HX, Wang JX, Zhang ZB, Le Y, Shen ZG, Chen JF. Micronization of atorvastatin calcium by antisolvent precipitation process. *Int J Pharm* 2009;**374**:106–13.

58. Zhang JY, Shen ZG, Zhong J, Hu TT, Chen JF, Ma ZQ, et al. Preparation of amorphous cefuroxime axetil nanoparticles by controlled nanoprecipitation method without surfactants. *Int J Pharm* 2006;**323**:153–60.

59. Sinha B, Müller RH, Möschwitzer JP. Bottom-up approaches for preparing drug nanocrystals: formulations and factors affecting particle size. *Int J Pharm* 2013;**453**:126–41.

60. Kumar V, Prud'homme RK. Nanoparticle stability: processing pathways for solvent removal. *Chem Eng Sci* 2009;**64**:1358–61.

61. Cheng KK, Yeung CF, Ho SW, Chow SF, Chow AH, Baum L. Highly stabilized curcumin nanoparticles tested in an *in vitro* blood–brain barrier model and in Alzheimer's disease Tg2576 mice. *AAPS J* 2013;**15**:324–36.

62. Yamasaki K, Kwok PC, Fukushige K, Prud'homme RK, Chan HK. Enhanced dissolution of inhalable cyclosporine nano-matrix particles with mannitol as matrix former. *Int J Pharm* 2011;**420**:34–42.

63. D'Addio SM, Kafka C, Akbulut M, Beattie P, Saad W, Herrera M, et al. Novel method for concentrating and drying polymeric nanoparticles: hydrogen bonding coacervate precipitation. *Mol Pharm* 2010;**7**:557–64.

64. Dalvi SV, Dave RN. Analysis of nucleation kinetics of poorly water-soluble drugs in presence of ultrasound and hydroxypropyl methyl cellulose during antisolvent precipitation. *Int J Pharm* 2010;**387**:172–9.

65. Liu Y, Kathan K, Saad W, Prud'homme RK. Ostwald ripening of *β*-carotene nanoparticles. *Phys Rev Lett* 2007;**98**:036102.

66. Wei Y, Dattachowdhury B, Vangara KK, Patel N, Alexander K, Boddu SH. Excipients that facilitate amorphous drug stabilization. In: Narang AS, Boddu SH, editors. *Excipient applications in formulation design and drug delivery.* Cham: Springer; 2015. p. 463–95.

67. Al-Obaidi H, Majumder M, Bari F. Amorphous and crystalline particulates: challenges and perspectives in drug delivery. *Curr Pharm Des* 2017;**23**:350–61.

68. Matteucci ME, Brettmann BK, Rogers TL, Elder EJ, Williams III RO, Johnston KP. Design of potent amorphous drug nanoparticles for rapid generation of highly supersaturated media. *Mol Pharm* 2007;**4**:782–93.

69. Dong Y, Ng WK, Shen S, Kim S, Tan RB. Preparation and characterization of spironolactone nanoparticles by antisolvent precipitation. *Int J Pharm* 2009;**375**:84–8.

70. Zhu W, Romanski FS, Meng X, Mitra S, Tomassone MS. Atomistic simulation study of surfactant and polymer interactions on the surface of a fenofibrate crystal. *Eur J Pharm Sci* 2011;**42**:452–61.

71. Van Eerdenbrugh B, Vermant J, Martens JA, Froyen L, Van Humbeeck J, Augustijns P, et al. A screening study of surface stabilization during the production of drug nanocrystals. *J Pharm Sci* 2009;**98**:2091–103.

72. Ross S, Morrison ED. *Colloidal systems and interfaces.* New York: Wiley; 1988.

73. Duro R, Souto C, Gómez-Amoza JL, Martínez-Pacheco R, Concheiro A. Interfacial adsorption of polymers and surfactants: implications for the properties of disperse systems of pharmaceutical interest. *Drug Dev Ind Pharm* 1999;**25**:817–29.

74. Verma S, Huey BD, Burgess DJ. Scanning probe microscopy method for nanosuspension stabilizer selection. *Langmuir* 2009;**25**:12481–7.

75. Letchford K, Burt H. A review of the formation and classification of amphiphilic block copolymer nanoparticulate structures: micelles, nanospheres, nanocapsules and polymersomes. *Eur J Pharm Biopharm* 2007;**65**:259–69.

76. Pattekari P, Zheng Z, Zhang X, Levchenko T, Torchilin V, Lvov Y. Top-down and bottom-up approaches in production of aqueous nanocolloids of low solubility drug paclitaxel. *Phys Chem Chem Phys* 2011;**13**:9014–9.

77. Yadav KS, Chuttani K, Mishra AK, Sawant KK. Long circulating nanoparticles of etoposide using PLGA-MPEG and PLGA-pluronic block copolymers: characterization, drug-release, blood-clearance, and biodistribution studies. *Drug Dev Res* 2010;**71**:228–39.

78. Anand P, Nair HB, Sung B, Kunnumakkara AB, Yadav VR, Tekmal RR, et al. RETRACTED: design of curcumin-loaded PLGA nanoparticles formulation with enhanced cellular uptake, and increased bioactivity *in vitro* and superior bioavailability *in vivo. Biochem Pharmacol* 2010;**79**:330–8.

79. Guhagarkar SA, Malshe VC, Devarajan PV. Nanoparticles of polyethylene sebacate: a new biodegradable polymer. *AAPS PharmSciTech* 2009;**10**:935–42.

80. Chorny M, Fishbein I, Danenberg HD, Golomb G. Lipophilic drug loaded nanospheres prepared by nanoprecipitation: effect of formulation variables on size, drug recovery and release kinetics. *J Controlled Release* 2002;**83**:389–400.

81. Dong Y, Feng SS. Methoxy poly(ethylene glycol)-poly(lactide) (mPEG-PLA) nanoparticles for controlled delivery of anticancer drugs. *Biomaterials* 2004;**25**:2843–9.

82. Legrand P, Lesieur S, Bochot A, Gref R, Raatjes W, Barratt G, et al. Influence of polymer behaviour in organic solution on the production of polylactide nanoparticles by nanoprecipitation. *Int J Pharm* 2007;**344**:33–43.

83. Kim S, Ng WK, Dong Y, Das S, Tan RB. Preparation and physicochemical characterization of *trans*-resveratrol nanoparticles by temperature-controlled antisolvent precipitation. *J Food Eng* 2012;**108**:37–42.

84. Matteucci ME, Paguio JC, Miller MA, Williams III RO, Johnston KP. Flocculated amorphous nanoparticles for highly supersaturated solutions. *Pharm Res* 2008;**25**:2477–87.

85. Zhang ZB, Shen ZG, Wang JX, Zhao H, Chen JF, Yun J. Nanonization of megestrol acetate by liquid precipitation. *Ind Eng Chem Res* 2009;**48**:8493–9.

86. Siddiqui SW, Zhao Y, Kukukova A, Kresta SM. Characteristics of a confined impinging jet reactor: energy dissipation, homogeneous and heterogeneous reaction products, and effect of unequal flow. *Ind Eng Chem Res* 2009;**48**:7945–58.

87. Marchisio DL, Rivautella L, Barresi AA. Design and scale-up of chemical reactors for nanoparticle precipitation. *AIChE J* 2006;**52**:1877–87.

88. Turino LN, Stella B, Dosio F, Luna JA, Barresi AA. Nanoparticles obtained by confined impinging jet mixer: poly (lactide-*co*-glycolide) *vs.* poly-ε-caprolactone. *Drug Dev Ind Pharm* 2018;**44**:934–41.

89. Massella D, Leone F, Peila R, Barresi AA, Ferri A. Functionalization of cotton fabrics with polycaprolactone nanoparticles for transdermal release of melatonin. *J Funct Biomater* 2018;**9**:1.

90. Ferri A, Kumari N, Peila R, Barresi AA. Production of menthol-loaded nanoparticles by solvent displacement. *Can J Chem Eng* 2017;**95**:1690–706.

91. Zhang Y, Feng J, McManus SA, Lu HD, Ristroph KD, Cho EJ, et al. Design and solidification of fast-releasing clofazimine nanoparticles for treatment of cryptosporidiosis. *Mol Pharm* 2017;**14**:3480–8.

92. Wang M, Xu Y, Wang J, Liu M, Yuan Z, Chen K, et al. Biocompatible nanoparticle based on dextran-*b*-poly(L-lactide) block copolymer formed by flash nanoprecipitation. *Chem Lett* 2015;**44**:1688–90.

93. Zhu Z. Effects of amphiphilic diblock copolymer on drug nanoparticle formation and stability. *Biomaterials* 2013;**34**:10238–48.

94. Fu Z, Li L, Wang M, Guo X. Size control of drug nanoparticles stabilized by mPEG-*b*-PCL during flash nanoprecipitation. *Colloid Polym Sci* 2018;**296**:935–40.

95. Luo H, Raciti D, Wang C, Herrera-Alonso M. Macromolecular brushes as stabilizers of hydrophobic solute nanoparticles. *Mol Pharm* 2016;**13**:1855–65.

96. Sun L, Liu Z, Wang L, Cun D, Tong HH, Yan R, et al. Enhanced topical penetration, system exposure and anti-psoriasis activity of two particle-sized, curcumin-loaded PLGA nanoparticles in hydrogel. *J Controlled Release* 2017;**254**:44–54.

97. Szymusiak M, Hu X, Plata PA, Ciupinski P, Wang ZJ, Liu Y. Bioavailability of curcumin and curcumin glucuronide in the central nervous system of mice after oral delivery of nano-curcumin. *Int J Pharm* 2016;**511**:415–23.

98. Shen H, Hu X, Szymusiak M, Wang ZJ, Liu Y. Orally administered nanocurcumin to attenuate morphine tolerance: comparison between negatively charged PLGA and partially and fully PEGylated nanoparticles. *Mol Pharm* 2013;**10**:4546–51.

99. Chopra M, Jain R, Dewangan AK, Varkey S, Mazumder S. Design of curcumin loaded polymeric nanoparticles-optimization, formulation and characterization. *J Nanosci Nanotechnol* 2016;**16**:9432–42.

100. Dewangan AK, Varkey S, Mazumder S. *Synthesis ofcurcumin loaded CMCAB nanoparticles for treatment of rheumatoid arthritis. International conference on chemical, environmental and biological sciences (CEBS)*. Dubai: CEBS; 2015.

101. Dewangan AK, Perumal Y, Pavurala N, Chopra K, Mazumder S. Preparation, characterization and anti-inflammatory effects of curcumin loaded carboxymethyl cellulose acetate butyrate nanoparticles on adjuvant induced arthritis in rats. *J Drug Deliv Sci Technol* 2017;**41**:269–79.

102. Bi C, Miao XQ, Chow SF, Wu WJ, Yan R, Liao YH, et al. Particle size effect of curcumin nanosuspensions on cytotoxicity, cellular internalization, *in vivo* pharmacokinetics and biodistribution. *Nanomed-Nanotechnol Biol Med* 2017;**13**:943–53.

103. Cheng KK, Chan PS, Fan S, Kwan SM, Yeung KL, Wáng YX, et al. Curcumin-conjugated magnetic nanoparticles for detecting amyloid plaques in Alzheimer's disease mice using magnetic resonance imaging (MRI). *Biomaterials* 2015;**44**:155–72.

104. Suzuki H, Hamao S, Seto Y, Sato H, Wong J, Prud'homme RK, et al. New nano-matrix oral formulation of nanoprecipitated cyclosporine a prepared with multi-inlet vortex mixer. *Int J Pharm* 2017;**516**:116–9.

105. Leung SS, Wong J, Guerra HV, Samnick K, Prud'homme RK, Chan HK. Porous mannitol carrier for pulmonary delivery of cyclosporine a nanoparticles. *AAPS J* 2017;**19**:578–86.

106. Sato H, Suzuki H, Yakushiji K, Wong J, Seto Y, Prud'homme RK, et al. Biopharmaceutical evaluation of novel cyclosporine a nano-matrix particles for inhalation. *Pharm Res* 2016;**33**:2107–16.

107. Wang Y, Song J, Chow SF, Chow AH, Zheng Y. Particle size tailoring of ursolic acid nanosuspensions for improved anticancer activity by controlled antisolvent precipitation. *Int J Pharm* 2015;**494**:479–89.

108. Shen H, Banerjee AA, Mlynarska P, Hautman M, Hong S, Kapetanovic IM, et al. Enhanced oral bioavailability of a cancer preventive agent (SR13668) by employing polymeric nanoparticles with high drug loading. *J Pharm Sci* 2012;**101**:3877–85.

109. Lazzari S, Moscatelli D, Codari F, Salmona M, Morbidelli M, Diomede L. Colloidal stability of polymeric nanoparticles in biological fluids. *J Nanopart Res* 2012;**14**:920.

110. McDaniel DK, Jo A, Ringel-Scaia VM, Coutermarsh-Ott S, Rothschild DE, Powell MD, et al. Tips pentacene loaded PEO-PDLLA core-shell nanoparticles have similar cellular uptake dynamics in M1 and M2 macrophages and in corresponding *in vivo* microenvironments. *Nanomed-Nanotechnol Biol Med* 2017;**13**:1255–66.

111. Mazumder S, Dewangan AK, Pavurala N. Enhanced dissolution of poorly soluble antiviral drugs from nanoparticles of cellulose acetate based solid dispersion matrices. *Asian J Pharm Sci* 2017;**12**:532–41.

112. Pereira JM, Mejia-Ariza R, Ilevbare GA, McGettigan HE, Sriranganathan N, Taylor LS, et al. Interplay of degradation, dissolution and stabilization of clarithromycin and its amorphous solid dispersions. *Mol Pharm* 2013;**10**:4640–53.

113. Chen T, Li C, Li Y, Yi X, Wang R, Lee SM, et al. Small-sized Mpeg-PLGA nanoparticles of schisantherin a with sustained release for enhanced brain uptake and anti-parkinsonian activity. *ACS Appl Mater Interfaces* 2017;**9**:9516–27.

114. Fang RH, Chen KN, Aryal S, Hu CM, Zhang K, Zhang L. Large-scale synthesis of lipid–polymer hybrid nanoparticles using a multi-inlet vortex reactor. *Langmuir* 2012;**28**:13824–9.

115. Vippagunta SR, Brittain HG, Grant DJ. Crystalline solids. *Adv Drug Deliv Rev* 2001;**48**:3–26.

116. Cardew PT, Davey RJ. The kinetics of solvent-mediated phase transformations. *Proc Roy Soc London Ser A-Mathem Phys Sci* 1985;**398**:415–28.

117. Greco K, Bogner R. Solution-mediated phase transformation: significance during dissolution and implications for bioavailability. *J Pharm Sci* 2012;**101**:2996–3018.

118. Whitesides GM. The origins and the future of microfluidics. *Nature* 2006;**442**:368–73.

119. Dittrich PS, Tachikawa K, Manz A. Micro total analysis systems. Latest advancements and trends. *Anal Chem* 2006;**78**:3887–908.

120. Zhao H, Wang JX, Wang QA, Chen JF, Yun J. Controlled liquid antisolvent precipitation of hydrophobic pharmaceutical nanoparticles in a microchannel reactor. *Ind Eng Chem Res* 2007;**46**:8229–35.

121. Ehrfeld W, Golbig K, Hessel V, Löwe H, Richter T. Characterization of mixing in micromixers by a test reaction: single mixing units and mixer arrays. *Ind Eng Chem Res* 1999;**38**:1075–82.

122. Sun J, Xianyu Y, Li M, Liu W, Zhang L, Liu D, et al. A microfluidic origami chip for synthesis of functionalized polymeric nanoparticles. *Nanoscale* 2013;**5**:5262–5.

123. Ali HS, York P, Blagden N. Preparation of hydrocortisone nanosuspension through a bottom-up nanoprecipitation technique using microfluidic reactors. *Int J Pharm* 2009;**375**:107–13.

124. Ali HS, York P, Ali AM, Blagden N. Hydrocortisone nanosuspensions for ophthalmic delivery: a comparative study between microfluidic nanoprecipitation and wet milling. *J Controlled Release* 2011;**149**:175–81.

125. Wang JX, Zhang QX, Zhou Y, Shao L, Chen JF. Microfluidic synthesis of amorphous cefuroxime axetil nanoparticles with size-dependent and enhanced dissolution rate. *Chem Eng J* 2010;**162**:844–51.

126. Zhang HX, Wang JX, Shao L, Chen JF. Microfluidic fabrication of monodispersed pharmaceutical colloidal spheres of atorvastatin calcium with tunable sizes. *Ind Eng Chem Res* 2010;**49**:4156–61.

127. Liu Z, Huang Y, Jin Y, Cheng Y. Mixing intensification by chaotic advection inside droplets for controlled nanoparticle preparation. *Microfluid Nanofluid* 2010;**9**:773–86.

128. Génot V, Desportes S, Croushore C, Lefèvre JP, Pansu RB, Delaire JA, et al. Synthesis of organic nanoparticles in a 3D flow focusing microreactor. *Chem Eng J* 2010;**161**:234–9.

129. Capretto L, Carugo D, Cheng W, Hill M, Zhang X. Continuous-flow production of polymeric micelles in microreactors: experimental and computational analysis. *J Colloid Interface Sci* 2011;**357**:243–51.

130. Capretto L, Mazzitelli S, Brognara E, Lampronti I, Carugo D, Hill M, et al. Mithramycin encapsulated in polymeric micelles by microfluidic technology as novel therapeutic protocol for β-thalassemia. *Int J Nanomed* 2012;**7**:307–24.

131. Capretto L, Mazzitelli S, Colombo G, Piva R, Penolazzi L, Vecchiatini R, et al. Production of polymeric micelles by microfluidic technology for combined drug delivery: application to osteogenic differentiation of human periodontal ligament mesenchymal stem cells (hPDLSCs). *Int J Pharm* 2013;**440**:195–206.

132. Capretto L, Cheng W, Carugo D, Katsamenis OL, Hill M, Zhang X. Mechanism of co-nanoprecipitation of organic actives and block copolymers in a microfluidic environment. *Nanotechnology* 2012;**23**:375602.

133. Hasani-Sadrabadi MM, Majedi FS, VanDersarl JJ, Dashtimoghadam E, Ghaffarian SR, Bertsch A, et al. Morphological tuning of polymeric nanoparticles *via* microfluidic platform for fuel cell applications. *J Am Chem Soc* 2012;**134**:18904–7.

134. Karnik R, Gu F, Basto P, Cannizzaro C, Dean L, Kyei-Manu W, et al. Microfluidic platform for controlled synthesis of polymeric nanoparticles. *Nano Lett* 2008;**8**:2906–12.

135. Zhang S, Yun J, Shen S, Chen Z, Yao K, Chen J, et al. Formation of solid lipid nanoparticles in a microchannel system with a cross-shaped junction. *Chem Eng Sci* 2008;**63**:5600–5.

136. Yun J, Zhang S, Shen S, Chen Z, Yao K, Chen J. Continuous production of solid lipid nanoparticles by liquid flow-focusing and gas displacing method in microchannels. *Chem Eng Sci* 2009;**64**:4115–22.

137. Jahn A, Vreeland WN, Gaitan M, Locascio LE. Controlled vesicle self-assembly in microfluidic channels with hydrodynamic focusing. *J Am Chem Soc* 2004;**126**:2674–5.

138. Dev S, Toster J, Prasanna SV, Fitzgerald M, Iyer KS, Raston CL. Suppressing regrowth of microfluidic generated drug nanocrystals using polyelectrolyte coatings. *RSC Adv* 2013;**3**:695–8.

139. Anton N, Bally F, Serra CA, Ali A, Arntz Y, Mely Y, et al. A new microfluidic setup for precise control of the polymer nanoprecipitation process and lipophilic drug encapsulation. *Soft Matter* 2012;**8**:10628–35.

140. Bally F, Garg DK, Serra CA, Hoarau Y, Anton N, Brochon C, et al. Improved size-tunable preparation of polymeric nanoparticles by microfluidic nanoprecipitation. *Polymer* 2012;**53**:5045–51.

141. Rhee M, Valencia PM, Rodriguez MI, Langer R, Farokhzad OC, Karnik R. Synthesis of size-tunable polymeric nanoparticles enabled by 3D hydrodynamic flow focusing in single-layer microchannels. *Adv Mater* 2011;**23**:H79–83.

142. Valencia PM, Basto PA, Zhang L, Rhee M, Langer R, Farokhzad OC, et al. Single-step assembly of homogenous lipid–polymeric and lipid–quantum dot nanoparticles enabled by microfluidic rapid mixing. *ACS Nano* 2010;**4**:1671–9.

143. Kim Y, Chung BL, Ma M, Mulder WJ, Fayad ZA, Farokhzad OC, et al. Mass production and size control of lipid–polymer hybrid nanoparticles through controlled microvortices. *Nano Lett* 2012;**12**:3587–91.

144. Chastek TQ, Iida K, Amis EJ, Fasolka MJ, Beers KL. A microfluidic platform for integrated synthesis and dynamic light scattering measurement of block copolymer micelles. *Lab Chip* 2008;**8**:950–7.

145. Chastek TQ, Beers KL, Amis EJ. Miniaturized dynamic light scattering instrumentation for use in microfluidic applications. *Rev Sci Instrum* 2007;**78**:072201.

146. Vladisavljević GT, Khalid N, Neves MA, Kuroiwa T, Nakajima M, Uemura K, et al. Industrial lab-on-a-chip: design, applications and scale-up for drug discovery and delivery. *Adv Drug Deliv Rev* 2013;**65**:1626–63.

147. Li W, Greener J, Voicu D, Kumacheva E. Multiple modular microfluidic (M³) reactors for the synthesis of polymer particles. *Lab Chip* 2009;**9**:2715–21.

148. Nisisako T, Torii T. Microfluidic large-scale integration on a chip for mass production of monodisperse droplets and particles. *Lab Chip* 2008;**8**:287–93.